Plastic deformation, vacancy diffusion, and vacancy delocalization in bcc ^{3}He

M. B. Manning, M. J. Moelter, and C. Elbaum
Metals Research Laboratory and Department of Physics, Brown University, Providence, Rhode Island 02912
(Received 8 July 1985)

The plastic deformation of bcc ^{3}He crystals has been studied near the melting curve, in the temperature range 0.65 K $\leq T \leq$ 1.17 K, and for strain rates, $\dot{\epsilon}$, from 2×10^{-6} to 2×10^{-4} sec^{-1}. The resulting relations between strain rate and stress, at a given temperature, are accounted for in terms of dislocation climb and vacancy diffusion in the solid He. The temperature dependence of the strain rate at a given stress indicates that a nonclassical mechanism underlies the deformation process. The vacancy diffusion coefficient in bcc ^{3}He, as a function of temperature, is deduced from these results, and an energy bandwidth for delocalized vacancies of 0.24±0.05 K is obtained through a fit to theoretical predictions.

I. INTRODUCTION

The study of defects in solid helium is motivated largely by the possibility that any defect in a quantum solid may become a delocalized excitation which can move with little hindrance through the crystal. In this context, there have been many theoretical investigations[1–4] of such effects as they apply to impurity atoms, vacancies, and dislocations in solid helium. Much of the earlier experimental work, however, has been carried out for the case of impurity atoms, typically small concentrations of ^{3}He in ^{4}He. In this case the motion of the ^{3}He impurity can be studied by NMR techniques[5,6] and its delocalized nature has been fairly well established.[6] Experimental studies of the behavior of other defects in quantum solids have followed more recently and in some of these plastic deformation has played a major role.[7–12]

Plastic flow in classical crystalline solids may be understood in terms of the motion of dislocations within the solid under an applied stress.[13] Impurity atoms, intersections with immobile (network) dislocations, and the Peierls potential are examples of obstacles to dislocation motion. The mechanisms by which the dislocations of a crystal overcome such barriers determine the rate of crystal deformation under stress. An investigation of plastic flow, the temperature dependence of the crystal strain rate under constant stress in particular, provides a means for the study of crystal defects which mediate these processes. Examples of such defect involvement in plastic deformation are the formation of dislocation double kinks by thermal activation or tunneling of the Peierls barrier (dislocation glide) and dislocation climb controlled by vacancy diffusion.[13]

In the case of quantum solids, plastic flow studies may explicitly verify the quantum-mechanical tunneling behavior of point defects (e.g., vacancies and dislocation kinks[3]), where unambiguous evidence of such delocalization effects from other kinds of experiments is not available.

Several investigations of plastic flow in solid He, previous to the present study, have been made. In the case of hcp ^{4}He, plastic flow appears to proceed by thermally activated dislocation motion.[7–10] Plastic flow in the bcc phases of ^{3}He and ^{4}He, however, has been both less thoroughly investigated and less readily attributable to dislocation slip than in the case of the hcp ^{4}He.[11,14] In fact, it has been proposed, on the basis of the small ultrasonic attenuation increases and evidence for localized deformation in bcc ^{4}He during its deformation,[11] that the role of dislocation slip in this process is secondary, at least in the usual (classical) sense. This is in contrast to the behavior of dislocations to hcp ^{4}He deformation, as determined by large ultrasonic attenuation increases while deformation proceeds.[10] In the bcc phases of the He solids the diffusion of mobile vacancies is considered to be a possible mechanism for mass flow.[11–15] It is precisely in such diffusion processes that the quantum nature of the He solids is expected to be most evident.

One of the objectives of the present study was to investigate plastic flow in bcc ^{3}He in a manner similar to the bcc ^{4}He plasticity experiments of Sanders *et al.*[11] In the present experiment it was found that stress-strain curves of bcc ^{3}He were quite distinct from those of hcp ^{4}He and very similar to those of bcc ^{4}He. It was not possible, however, to satisfactorily account for the relationship between the flow stress and the strain rate in bcc ^{3}He over the temperature range investigated by either a vacancy diffusion mass transport or by classical dislocation slip motion alone. Instead, a model involving both of these mechanisms gives good agreement with the experimental results and yields a value for the bandwidth of delocalized vacancies.

II. APPARATUS AND EXPERIMENTAL TECHNIQUES

A. Apparatus

The apparatus used in these experiments is depicted in Fig. 1. The sample space was circular with a cross sectional area of $\approx$1.8 cm^2 and a height of $\approx$1.7 cm. Three mutually perpendicular pairs of $LiNbO_3$ transducers, having resonant frequencies of 5 and 10 MHz for the two horizontal directions, and 10 MHz for the vertical direc-

tion of wave propagation, were situated in the sample cell as indicated. Pulsed ultrasonic waves at these frequencies were used to monitor features of crystal growth and deformation. The He crystals were deformed by a piston which was positioned in the upper part of the cell and made mobile by CuBe bellows. In order to make the deformation measurements, the piston, ordinarily forced to the top of the cell due to the large pressure ($\approx$50 atm) of the ^{3}He sample, was freed by pressurizing with ^{4}He, a volume containing bellows counteracting the cell pressure. A large (100 l) ^{4}He ballast volume, held at an appropriate pressure (8—10 atm), was connected to this ^{4}He counteracting bellows space. The additional force necessary to deform the crystal was provided by a tubular, stainless-steel shaft driven mechanically downward at a controlled rate. At the bottom of this shaft, a three pronged coupling, circumventing the upper bellows volume, was attached to the drive shaft of the piston. The piston displacement (proportional to crystal strain) was measured by the lower strain ring which was secured to the top of the cryostat and to the top of the drive shaft. The applied force (proportional to the stress on the crystal) was measured by a strain ring placed at the top of the mechanical deformation driveshaft.

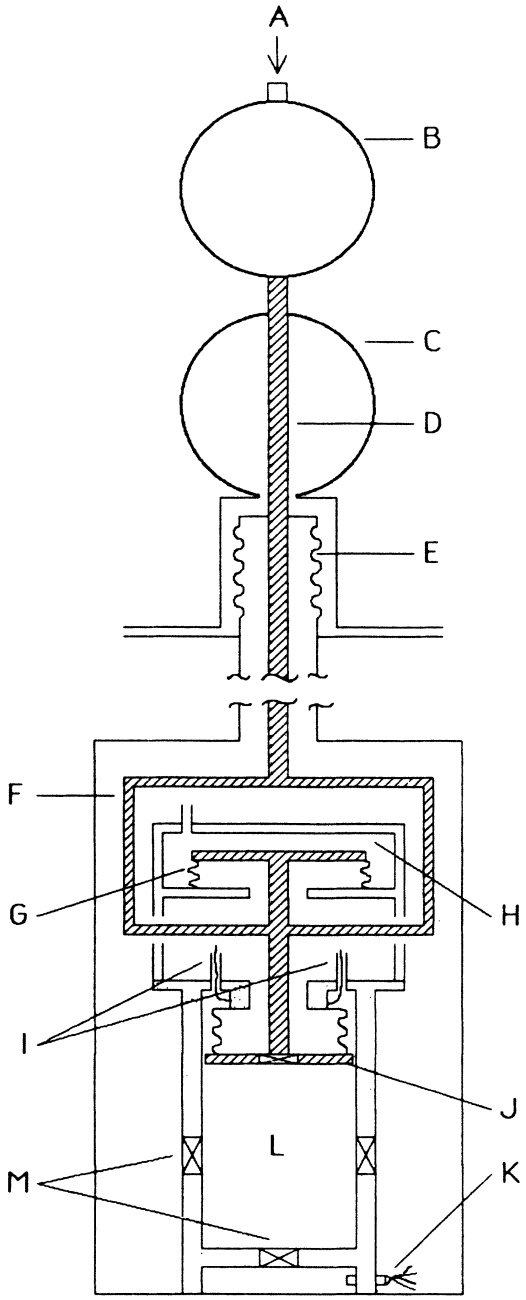

FIG. 1. Sample cell and deformation apparatus. *A*, applied force; *B*, force (stress) ring; *C*, displacement (strain) ring; *D*, deformation shaft; *E*, bellows; *F*, deformation shaft with coupling to circumvent counteracting bellows volume; *G*, counteracting bellows; *H*, counteracting bellows volume (^{4}He); *I*, sample space fill lines with heaters (^{3}He); *J*, deforming piston; *K*, germanium thermometer; *L*, sample space (^{3}He); *M*, ultrasonic transducers.

Stress- and strain-ring calibrations were performed at the beginning and end of the present study. The stress-ring calibrations agreed to better than 1% and those of the strain rings agreed to 1.5%.

B. ^{3}He crystal growth and quality

High-quality bcc ^{3}He crystals are most reliably grown under constant pressure conditions.[16] However, due to the high cost of ^{3}He, it is impractical to use a constant pressure provided by a large ballast volume. The following method was therefore developed for growing ^{3}He crystals under nearly isobaric conditions (see Fig. 2). During the transfer of liquid ^{4}He into the main Dewar, a pressurized volume (16 atm, $\approx$0.45 liters) of ^{3}He gas was opened to the sample cell. At the completion of the liquid-^{4}He transfer, the sample cell was valved shut and a 9-cc stainless-steel volume ("bomb") filled with molecular sieve[17] (Linde 13x) was opened to the remaining ^{3}He gas in the storage volume. The bomb was then cooled to 4.2

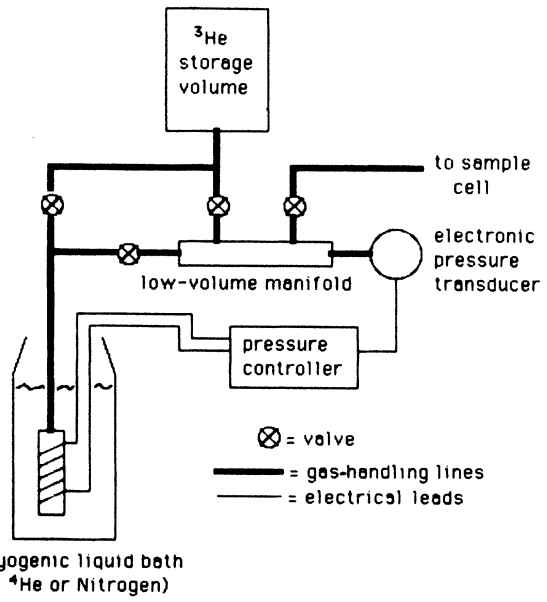

FIG. 2. Pressurization and pressure control system for bcc ^{3}He sample cell. For initial pressurization, liquid ^{4}He is used; for subsequent control, liquid N_2 is used.

K. The ^{3}He storage volume was closed and the bomb was withdrawn from the liquid-^{4}He bath slowly, pressurizing a low-volume gas-handling manifold connected to the sample cell. The pressure in this manifold was monitored by an electronic pressure transducer. (Setra Systems, Inc., Model No. 205-2.) No more than three such temperature cyclings of the bomb were necessary to obtain cell pressures in excess of 60 atm. In order to grow a crystal at a given pressure, the pressurization bomb was placed in a liquid-N_2 bath with ^{3}He pressure in the bomb $\approx 15\%$ in excess of the anticipated growth pressure. The pressurization bomb was then valved shut. Next the ^{3}He pressure in the sample cell was reduced to a value 2—5 % in excess of the growth pressure. The initial cooling of the sample cell from 4.2 K began by pumping on the liquid-^{4}He bath and continued with ^{3}He refrigeration. As the ^{3}He melting curve[18] was approached, the cell pressure was adjusted to the appropriate value. The onset of solidification was determined by the behavior of the vertical ultrasonic signals and verified by the known temperature and pressure on the melting curve.[18] The overpressure in the bomb was used for the first one-third of the crystal growth by careful bleeding of the ^{3}He gas out of the pressure bomb. When the bomb overpressurization had been exhausted, a pressure control system was enabled. This involved joule heating of the bomb according to a control circuit utilizing the output of the electronic pressure transducer, which measured the pressure at the gas-handling manifold. Using this system, pressure control was maintained to ± 0.003 atm as determined by the output of the pressure transducer. The crystals were grown in a vertical temperature gradient and this growth was monitored by observing the position of the solid-liquid interface by means of the ultrasonic signals.

For the bcc ^{3}He specimens grown in the present experiments the following facts suggest that single crystals have been grown.

(1) The crystal growth rates (1—2 cm/hr) were very close to those found to be optimal for high crystal quality in x-ray-diffraction experiments.[16–19]

(2) The ultrasonic velocities observed in three mutually orthogonal directions in the crystal were usually different by amounts well in excess of velocity resolution of the apparatus.

(3) The effects of apparent beam focusing[20] were frequently observed, whereby the ultrasonic signal in one horizontal direction in the solid was of very high quality with numerous echoes, and the other horizontal ultrasonic signal was not observable at all.

The orientations of these bcc ^{3}He samples, assuming that they were single crystals, were difficult to determine with the ultrasonic velocity resolution of the apparatus ($\approx 1\%$) even though distinct velocity values were observed in three orthogonal directions of the sample. This is because of degeneracies in the directional dependence of the ultrasonic velocities.[19] The completely grown bcc ^{3}He crystals remained in a temperature gradient during deformation. It was possible to estimate the size of these temperature gradients by noting that a liquid-solid ^{3}He interface existed in the cell at approximately the position of the crystal deforming piston (Fig. 1). Since the fill capillary was kept free of solid, the temperature of this interface could be determined by referring to the pressure and temperature values along the melting curve.[18] The thermal conductivity of bcc ^{3}He over the range of molar volumes used here was estimated according to published results.[21,22] By comparing the thermal conductivity of the bcc ^{3}He to the Kapitza resistance at the bcc ^{3}He-Cu boundary[23] at the base of the cell, an estimate of the thermal gradient in the crystal could be made. (We note that the thermometer is located at the base of the cell.) The result of this analysis was that the temperature differences between the top and the bottom of the bcc ^{3}He specimens ranged from 40 mK for crystals at 0.65 K to 65 mK for those at 1.17 K. The average values of thermal gradients were correspondingly, 24—36 mK/cm.

III. DATA ACQUISITION AND ANALYSIS

Over 100 crystals were grown for these experiments, more than half of which were not used for further analysis, usually for one or more of the following reasons: (1) the fill line to the sample cell, which allowed constant pressure conditions to exist for the crystal during deformation, had blocked; (2) loss of the vertical ultrasonic signal resulting in the inability to follow the position of the solid-liquid interface; and (3) temperature or pressure control and stability was lost during the deformation.

Whether the sample-cell fill line was blocked or free was of particular importance for the interpretation of the data. An extensive testing effort was made therefore with two purposes: (1) to establish experimental techniques which dependably resulted in unblocked fill lines and (2) to identify behavior characteristic of a blocked fill line in order to recognize this situation should it inadvertently arise.

Deformations were monitored continuously by displaying stress and strain data as they were acquired. The stress and strain measurements on crystals deformed at a constant strain rate displayed the pattern shown in Fig. 3. At each selected temperature and pressure crystals were deformed at 2—4 strain rates by changing the speed of the mechanical drive to a higher value while a deformation was in progress. Liquid calibrations for each solid run were also carried out. The system parameters for the

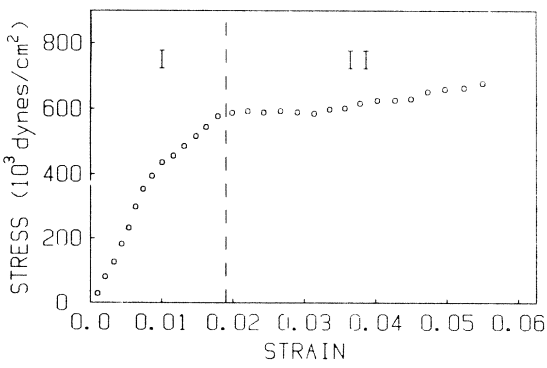

FIG. 3. Representative stress-strain curve for bcc ^{3}He crystals deformed plastically at 1 K.

liquid calibration run were made to correspond to those used during the solid run in every respect, including the deformation rates, the rate change points, and starting points.

A linear fit to the liquid points was then subtracted from the solid deformation data to display the characteristics of the plastic deformation of the solid alone. Corrections were also made for any recorded differences in the various pressure systems influencing the measurements, and for the other known systematic sources of error (e.g., shaft bending under the applied load).

General features of the plastic deformation curves for solid He were identified and analyzed. Figure 3 shows the two distinct (and repeatable) regions of plastic behavior for bcc ^{3}He. An initial period of deformation, the extent of which depended on the imposed strain rate (or applied stress) existed for all the bcc ^{3}He crystals tested. This region, labeled I in Fig. 3, terminated at a point where an abrupt change of slope in the stress-strain curve occurred. The increase in the stress beyond this point was usually less than 10% of the final value (region II). The average value of the stress in region II is defined as the flow stress, σ_f.

The following, general features of the bcc ^{3}He stress-strain curves[7–9] (Fig. 3) are noted. (1) Neither distinct yield points nor yield drops were seen in these curves, a result confirmed over the entire range of crystals and deformation rates investigated here. (2) No systematic evidence was found for significant strain hardening in bcc ^{3}He (i.e., $d\sigma/d\epsilon \simeq 0$ in region II where σ is the applied stress and ϵ is the strain). The lack of strain hardening in bcc ^{3}He has also been noted by Sakai *et al.*[14]

For studies of defect mobility in quantum solids the most important aspect of the bcc ^{3}He plastic deformation data is the relationship among flow stress, strain rate, and temperature. The temperatures used for these and later purposes are the average temperatures of these crystals defined previously. Figure 4 displays these data for two of the temperatures investigated. For each temperature the data were fit to an expression of the form

$$\dot{\epsilon} = A_0 + A_1\sigma_f + A_2\sigma_f^4 , \tag{1}$$

where A_0, A_1, and A_2 are fitting parameters and σ_f and $\dot{\epsilon}$ are the flow stress and strain rate, respectively. (See Table I.)

Figure 5 displays the temperature dependence of the strain rate at several fixed flow stresses. Of particular note here is the common trend of an initial rise to a broad maximum situated at ≈ 0.75 K for the lower applied stresses and ≈ 0.9 K for the higher stresses. These maxima are followed by a *decline* in the strain rate as the temperature increases. This decrease in the strain rate with increasing temperature is not found in the deformation of classical crystals. Vertical and horizontal ultrasonic signals were monitored throughout the deformation process. It was observed that the vertical ultrasonic attenuation increased as the crystals were strained. This attenuation was greatest ($\lesssim 10$ db/cm) for the higher strain rates ($\dot{\epsilon} > 7\times 10^{-5}$/sec) and was reduced, to $\lesssim 3$ db/cm, for the lower strain rate ($\dot{\epsilon} < 10^{-5}$/sec). The horizontal ultrasonic attenuation was unchanged for low strain rates ($\dot{\epsilon} < 2\times 10^{-5}$/sec). However, at the highest strain rates a relatively small horizontal ultrasonic attenuation increase ($\lesssim 6$ db/cm) took place. These ultrasonic attenuation results are consistent with those found by Sanders *et al.*[11]—during the plastic deformation of bcc ^{4}He. We conclude from this attenuation behavior, that the mechanism of plastic deformation is localized to the region near the piston.

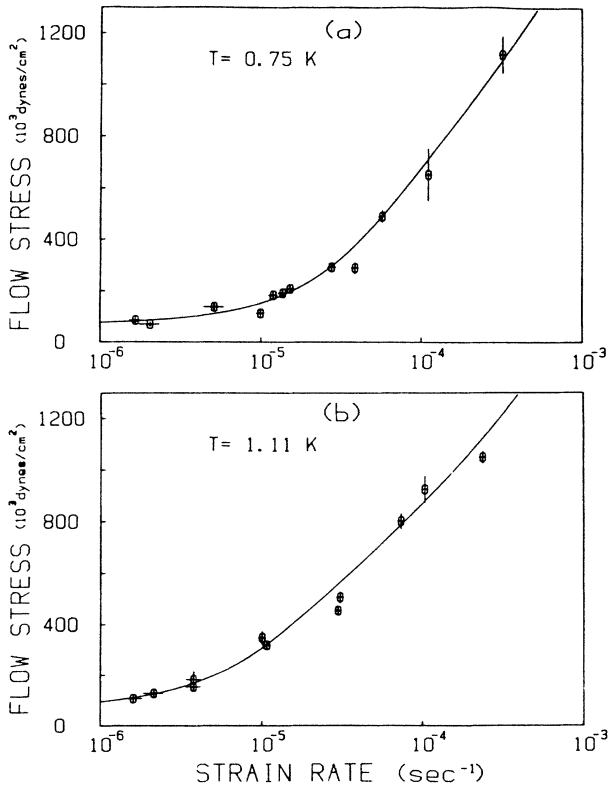

FIG. 4. Flow stress versus strain rate for bcc ^{3}He crystals at two of the temperatures investigated: (a) 0.75 K, (b) 1.11 K. The solid lines are the best fits of Eq. (1) with the values of the parameters listed in Table I.

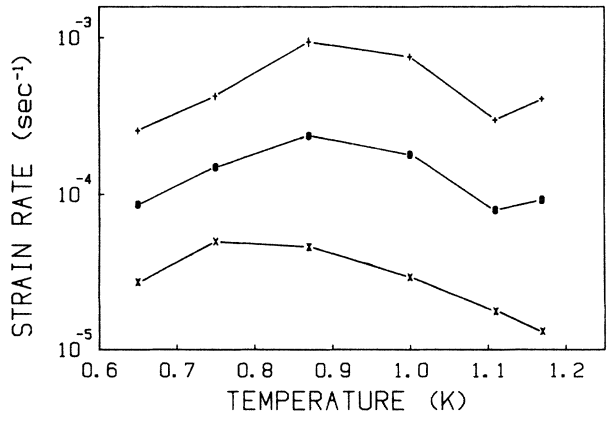

FIG. 5. Strain rate as a function of temperature for bcc ^{3}He crystals deformed at three different values of flow stress. ×, 4×10^5 dyn cm^{-2}; ⓪, 8×10^5 dyn cm^{-2}; +, 12×10^5 dyn cm^{-2}. The solid lines are guides to the eye.

TABLE I. Values of the parameters A_0, A_1, A_2, appearing in Eq. (1), for deformations at the six temperatures listed.

T (K)	A_0 10^{-6} sec^{-1}	A_1 10^{-11} sec^{-1} (dyn/cm^2)$^{-1}$	A_2 10^{-29} sec^{-1} (dyn/cm^2)$^{-4}$
0.65	0.92 (±0.23)	6.37 (±0.30)	8.58 (±0.53)
0.75	−7.83 (±0.32)	11.65 (±0.31)	13.7 (±1.01)
0.87	−3.66 (±0.55)	8.99 (±0.56)	40.0 (±2.9)
1.00	−1.90 (±0.34)	5.31 (±0.26)	33.3 (±1.6)
1.11	−2.45 (±0.31)	3.64 (±0.17)	12.3 (±0.54)
1.17	−0.93 (±0.15)	2.11 (±0.11)	18.5 (±0.70)

IV. DISCUSSION

Fundamental differences in the mass-transport behavior of the bcc and hcp structures of solid helium are apparent in the temperature dependences of the flow stress-strain rate behavior. In the case of hcp ^{4}He a classical Arrhenius-type temperature dependence of the strain rate at fixed flow stress is found.[7–9] In the bcc structures, as this study has shown for ^{3}He and that of Sanders *et al.*[15] for ^{4}He, the temperature dependence of the strain rate at fixed flow stress is nonclassical. In the present experiments the strain rate decreases with increasing temperature after going through a maximum, whereas in the bcc ^{4}He studies cited above the process was found to be athermal.

To account for the present data we consider both dislocation climb and vacancy diffusion. Equation (1), which was fitted to the flow stress-strain data, reflects these considerations. In previous plastic deformation experiments on solid He it has been observed that a minimum stress must be applied before plastic flow at observable rates ($\dot{\epsilon} \gtrsim 10^{-7}$/sec) occurs. The existence of such a minimum stress was generally indicated in the present experiments as well. Accordingly, a strain rate offset term, A_0, has been included in Eq. (1) to account for this minimum stress. The other terms are included on the assumption that plastic flow in bcc ^{3}He takes place by the diffusion of highly mobile vacancies in the solid. These vacancies originate both from the surface of the crystal and from climbing dislocations in the solid. Macroscopic mass transport in solid He (on experimental time scales) by the diffusion of vacancies has been previously conjectured by Andreev *et al.*[24] for the case of an imbedded metal sphere forced to move within solid helium. For bcc ^{4}He, qualitative (ultrasonic) evidence supporting this proposal has been offered by Sanders *et al.*[11] However, the latter authors note the possible role of dislocation climb in this process, where the former assume that vacancy accommodation takes place at the interface between the solid helium and the moving sphere. According to the Andreev view the vacancies travel in a sourceless medium driven by the gradient of the excess chemical potential, μ', which satisfies the equation $\nabla^2\mu'=0$. We found that to account for the present experimental data contributions from internal sources and sinks of vacancies to this process must be included. We postulate, therefore, that vacancy emission and absorption is associated with climbing dislocations. The mechanism of plastic flow proposed here is, therefore, closely related to the well-known phenomenon of the Nabarro-Herring creep.[25,26] The contribution to the observed crystal strain rate from vacancy diffusion between sources and sinks is proportional to the applied stress. It is of the following form:

$$\dot{\epsilon}=\frac{D}{k_B T}A_1'\sigma_f\ , \tag{2}$$

where $\dot{\epsilon}$ is the strain rate, σ_f the flow stress, and D, k_B, and T are the vacancy diffusion coefficient, Boltzmann's constant, and the temperature, respectively. A_1' is a constant containing quantities which depend on the sample and its geometry (for details see Appendix A). It has been previously found that the flow-stress-strain rate dependence of hcp ^{4}He (Refs. 7 and 8) and bcc ^{3}He (Ref. 14) may be accounted for by the Weertman creep.[27] This amounts to the problem of dislocation climb in the presence of topological barriers to their motion, in particular, immobile network dislocations. The expression for Weertman creep at moderate stresses is of the form

$$\dot{\epsilon}=\frac{D}{k_B T}A_2'\sigma_f^m\ , \tag{3}$$

where $\dot{\epsilon}$, σ_f, D, k_B, and T are defined as above. The constant A_2' contains quantities which depend on the sample and dislocation characteristics (for details see Appendix A). Values of the exponent m between 3.5 and 4.5 have been reported for classical solids. In the present analysis, $m=4$ has been chosen and is used in the third term in

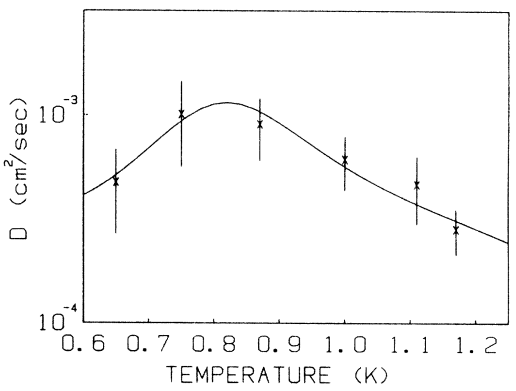

FIG. 6. Diffusion coefficient of vacancies in bcc ^{3}He versus temperature, derived from the experimental data as discussed in Appendix A. The solid line is a fit of the experimental data to Eq. (B1).

Eq. (1). This value of m yields a good fit to the experimental data.

In order to deduce D from these data, the experimental ratio, A_2/A_1, at each temperature and the expression for A_1 [Eq. (A1)] have been used. The results are displayed in Fig. 6. The decrease of the vacancy diffusion coefficient for bcc ^{3}He with increasing temperature clearly indicates the nonclassical nature of this process.

The quantum diffusion of vacancies in quantum crystals has been anticipated in several theoretical investigations of the problem. Andreev[3,4] has discussed the temperature dependence of point-defect diffusion (vacancies and impurities) in terms of delocalized quasiparticles that form an energy band, including their interaction with phonons. Kagan *et al.*[28–30] have also considered this problem with emphasis on the stability of the defect energy band in the presence of phonons and defect interactions. There are several qualitative results of these two treatments which are in agreement. However, the Kagan *et al.* theory predicts the existence of a broad maximum in the value of the diffusion coefficient as a function of temperature, under certain conditions.[31] Such a feature is found in the present data. The solid curve shown in Fig. 6 represents the quantity D according to an explicit expression for the diffusion of point defects in quantum crystals derived by Kagan *et al.*[29,30]

The Kagan *et al.* expression for the diffusion coefficient involves some parameters whose values are available[32] only for the case of ^{3}He atoms in hcp ^{4}He. The choices of these parameters made for the present study are discussed in Appendix B. We have analyzed our data, with these values, using the Kagan *et al.* expression [Eq. (B1)]. The analysis resulted in a vacancy bandwidth for bcc ^{3}He of 0.24 ± 0.05 K. This result compares favorably with values for the vacancy bandwidth reported on the basis of NMR experiments (≈ 0.4 K).[33]

We conclude from this procedure that the quantum diffusion of vacancies plays a critical role in the plastic flow of bcc ^{3}He. Furthermore, the data reviewed in this manner support the treatment of point-defect diffusion in quantum crystals given by Kagan *et al.*

V. SUMMARY

We have studied the plastic deformation of bcc ^{3}He crystals, near the melting curve, as a function of temperature and imposed strain rate. The resulting relations between stress, strain rate, and temperature are interpreted in terms of theoretical models involving dislocation climb and vacancy diffusion. The experimental results on the temperature dependence of the strain rate at constant stress provide a qualitative indication that the mechanism underlying the deformation process is nonclassical. The diffusion coefficient D, for vacancies in bcc ^{3}He, as a function of temperature, deduced from the above data also displays nonclassical behavior. D is then analyzed in terms of a model by Kagan *et al.* and the resulting fit yields a value for the energy bandwidth for vacancies of 0.24 ± 0.05 K, when existing values of the other parameters of the theory are used.

ACKNOWLEDGMENT

This research was supported by the National Science Foundation under Grant No. DMR-8304224.

APPENDIX A

In this appendix we present expressions for the coefficients A_1 and A_2 which appear in Eq. (1) [see also Eqs. (2) and (3)]. We also examine the present analysis for quantitative consistency in light of the experimentally determined values of A_1 and A_2 (see Table I).

The expression for A_1 corresponding to vacancy diffusion in the presence of vacancy sources and sinks is[25,26]

$$A_1 = DA_1'/k_BT = D\Omega_0 c/k_BTrd \ , \tag{A1}$$

where D is the vacancy diffusion coefficient, k_B is Boltzmann's constant, T is the temperature, Ω_0 is the atomic volume, r is the distance between vacancy sources and sinks, c is the vacancy concentration, and d is the height of the crystal (which relates the piston velocity to the crystal strain rate).

Following the treatment of Weertman,[27] the coefficient of the σ_f^4 term in Eq. (1) is

$$A_2 = DA_2'/k_BT = 30Db^3N_0LL'M\mathscr{L}^2/k_BT\mu^3 \ . \tag{A2}$$

Here D, k_B, and T are defined as above, b is the magnitude of the Burgers vector, N_0 is the number of vacancies per unit volume in the region between dislocation pile ups,[13] L is the distance which an edge dislocation moves after breaking away from the barrier, L' is the distance a screw dislocation moves after breakaway, M is the number of active Frank-Read sources per unit volume, $\mathscr{L}$ is the width of the piled-up dislocation group, and μ is the shear modulus.

We now compare the value of A_2/A_1 from Eqs. (A1) and (A2) with that obtained from experiment, taking $T=1.0$ K. From Eqs. (A1) and (A2) we find, in cgs units,

$$A_2/A_1 = 0.5LL'M\mathscr{L}^2 \ , \tag{A3}$$

where L, L', M, and $\mathscr{L}$ are defined as above and we have taken values of the remaining quantities appropriate to the conditions of the experiment and $T=1.0$ K. Specifically, $d=1.7$ cm, $c=0.005$ (see Appendix B), $N=1.26\times10^{20}$ cm^{-3}, $\Omega_0=3.9\times10^{-23}$ cm^3, $b=3.7\times10^{-8}$ cm, $r=10^{-2}$ cm, and $\mu=3.26\times10^7$ dyn/cm^2. Using the values in Table I for A_1 and A_2 we obtain

$$(A_2/A_1)_{\text{expt}} = 6\times10^{-18} \text{ cm}^6/\text{dyn}^3 \ . \tag{A4}$$

Agreement between theory and experiment can be obtained by taking $L\approx L'\approx10^{-5}$ cm, $M\approx10^5$ cm^{-3}, and $\mathscr{L}\approx10^{-6}$ cm. These values are consistent with other studies of dislocations in ^{3}He, e.g., Ref. 34. Similar values for the quantities L, L', M, and $\mathscr{L}$ are found when the preceding analysis is carried out for the other temperatures investigated.

APPENDIX B

Kagan *et al.*[28–30] have given an approximate expression for the diffusion coefficient D, for all defect concen-

trations and for the temperature range over which activated processes are insignificant. That expression is presented in this appendix [Eq. (B1)] along with the numerical values chosen for the various quantities used in our fitting of the data which appear in Fig. 6. The diffusion coefficient is given by

$$D=(za^2\Delta_0^2/3)(Q(x)/[\Omega_x+\Omega_{\rm ph}(T)] +[1-Q(x)]\Omega_{\rm ph}(T)/\{[\delta\epsilon(x)]^2 +[\Omega_{\rm ph}(T)]^2\}) . \quad \text{(B1)}$$

(In the above expression and those which follow $k_B=1$, $\hbar=1$.) Here, z is the coordination number, Δ_0 is the tunneling amplitude, a is the interparticle spacing, x is the concentration of the diffusing entity, and T is the temperature. The functions are defined in the following manner.

(a) $Q(x)=[(x^c-x)/x^c]^t$, where x^c is a parameter of the theory referred to by the authors as a critical concentration.

(b) $\Omega_x=a\Delta(x/a^3)\pi r^2$, with a and x as above, Δ is the energy bandwidth ($\Delta=z\Delta_0$), πr^2 is an effective cross section subject to the condition $r=a(U_0/\Delta)^{1/3}$, and U_0 is the defect-defect interaction strength according to the relation $\epsilon(r)=U_0(a/r)^3$.

(c) $\Omega_{\rm ph}(T)=10^6B(T/\Theta_D)^9\Theta_D$, where B is a constant of order unity, and Θ_D is the Debye temperature.

(d) $\delta\epsilon(x)=\alpha U_0x^{4/3}$ with x and U_0 as before, and α a constant of order unity.

For the present study we have used $a=3.7$ Å,[35] $\Theta_D=15$ K,[36] and $z=8$ for the coordination number of the bcc phase. Based on recent measurements of vacancy concentration along the melting curve[37] we take $x=0.005$ for the concentration. Values for the remaining quantities appearing in Eq. (B1) are not presently available for the case of vacancy diffusion in bcc ^{3}He. Using results obtained by Mikheev *et al.*[32] for the case of ^{3}He impurities diffusing in hcp ^{4}He we take $\alpha=0.35$, $B=0.22$, and the exponent $t=1.7$. With these choices, the remaining quantities U_0, Δ_0, and x^c were taken as free parameters for the fitting of Eq. (B1) to the data shown in Fig. 6. The solid line is the result of the fit with the following values: $U_0=0.048$ (±0.022) K, $\Delta_0=0.03$ (±0.006) K [note that $\Delta=z\Delta_0=0.24$ (±0.05) K is the vacancy energy bandwidth], and $x^c=0.15$ (±0.11) is the critical concentration.

[1] A. F. Andreev and I. M. Lifshitz, Zh. Eksp. Teor. Fiz. **56**, 2057 (1969) [Sov. Phys.—JETP **29**, 1107 (1969)].

[2] R. A. Guyer, R. C. Richardson, and L. I. Zane, Rev. Mod. Phys. **43**, 532 (1971).

[3] A. F. Andreev, Usp. Fiz. Nauk **118**, 251 (1976) [Sov. Phys.—Usp. **19**, 137 (1976)].

[4] A. F. Andreev, in *Progress in Low Temperature Physics*, edited by D. F. Brewer (North-Holland, Amsterdam, 1982), Chap. II, p. 69.

[5] M. G. Richards, J. Pope, and A. Widom, Phys. Rev. Lett. **29**, 708 (1972).

[6] A. R. Allen and M. G. Richards, Phys. Lett. **65A**, 36 (1978).

[7] H. Suzuki, J. Phys. Soc. Jpn. **35**, 1472 (1973).

[8] V. L. Tsymbalenko, Pis'ma Zh. Eksp. Teor. Fiz. **23**, 709 (1976) [JETP Lett. **23**, 653 (1977)].

[9] H. Suzuki, J. Phys. Soc. Jpn. **42**, 1865 (1977).

[10] D. J. Sanders, H. Kwun, A. Hikata, and C. Elbaum, Phys. Rev. Lett. **39**, 815 (1977).

[11] D. J. Sanders, H. Kwun, A. Hikata, and C. Elbaum, Phys. Rev. Lett. **40**, 458 (1978).

[12] I. Iwasa, N. Saito, and H. Suzuki, J. Phys. Soc. Jpn. **52**, 952 (1982).

[13] F. R. N. Nabarro, *Theory of Crystal Dislocation* (Oxford University, New York, 1967).

[14] A. Sakai, Y. Nishioka, and H. Suzuki, J. Phys. Soc. Jpn. **46**, 881 (1979).

[15] D. J. Sanders, H. Kwun, A. Hikata, and C. Elbaum, J. Low Temp. Phys. **35**, 221 (1979).

[16] B. A. Fraass, S. M. Heald, and R. O. Simmons, J. Cryst. Growth **42**, 370 (1977).

[17] D. S. Greywall, Phys. Rev. B **15**, 2604 (1977).

[18] E. R. Grilly, J. Low Temp. Phys. **11**, 33 (1973).

[19] D. S. Greywall, Phys. Rev. A **3**, 2106 (1971).

[20] R. Wanner, Phys. Rev. A **3**, 448 (1971).

[21] W. C. Thomlinson, J. Low Temp. Phys. **9**, 167 (1972).

[22] A. S. Greenberg and G. Armstrong, Phys. Rev. B **20**, 1050 (1979).

[23] L. P. Mezhov-Deglin, Zh. Eksp. Teor. Fiz. **71**, 1453 (1977) [Sov. Phys.—JETP **44**, 761 (1977)].

[24] A. F. Andreev, K. Keshishev, L. Mezhov-Deglin, and A. Shalnikov, Pis'ma Zh. Eksp. Teor. Fiz. **9**, 507 (1969) [JETP Lett. **9**, 306 (1969)].

[25] C. Herring, J. Appl. Phys. **21**, 437 (1950).

[26] I. M. Lifshitz, Zh. Eksp. Teor. Fiz. **43**, 1281 (1962) [Sov. Phys.—JETP **17**, 909 (1963)].

[27] J. Weertman, J. Appl. Phys. **29**, 1685 (1958).

[28] Yu. Kagan, in *Defects in Insulating Crystals Proceedings of the International Conference, Riga, May, 1981*, edited by V. M. Iuehkevich and K. K. Shvarts (Springer, New York, 1981).

[29] Yu. Kagan and L. A. Maksimov, Zh. Eksp. Teor. Fiz. **84**, 792 (1983) [Sov. Phys.—JETP **57**, 459 (1983)].

[30] Yu. Kagan and L. A. Maksimov, Phys. Lett. **95A**, 242 (1983).

[31] We have examined the consequences on the vacancy diffusion coefficient values obtained here, of assuming differences in vacancy concentration at different temperatures corresponding to the extremes of the values reported by Heald *et al.* (Ref. 37) within the temperature range of our experiments. Thus, we have found that the salient feature, namely, the maximum of the diffusion coefficient as a function of temperature, persists and is not attributable, therefore, to variations of vacancy concentration within the limits of available data.

[32] V. A. Mikheev, V. A. Maidanov, and N. P. Mikhin, Solid State Commun. **48**, 361 (1983).

[33] N. Sullivan, G. Deville, and A. Landesman, Phys. Rev. B **11**, 1858 (1975).

[34] J. R. Beamish and J. P. Franck, Phys. Rev. B **26**, 6104 (1982).

[35] W. E. Keller, *Helium-3 and Helium-4* (Plenum, New York, 1969), Chap. 9.

[36] J. Wilks, *The Properties of Liquid and Solid Helium* (Clarendon, Oxford, 1967), Chap. 22.

[37] S. M. Heald, D. R. Baer, and R. O. Simmons, Phys. Rev. B **30**, 2531 (1984).